Journal of Materials Chemistry A

Accepted Manuscript

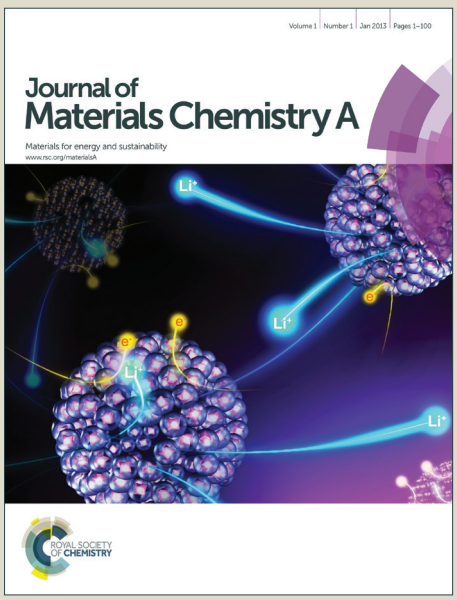

ROYAL SOCIETY OF CHEMISTRY

www.rsc.org/materialsA

table of contents only

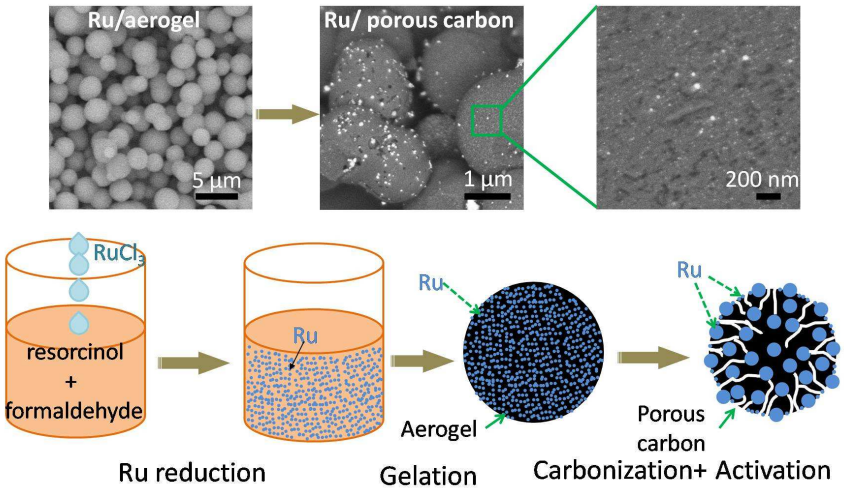

Cite this: DOI: 10.1039/c0xx00000x

www.rsc.org/xxxxxx

ARTICLE TYPE

Preparation of Porous Carbon with High Dispersion of Ru Nanoparticles by Sol-gel Method and Its Application in Hydrogen Storage

Yuanzhen Chen, Yongning Liu*

Received (in XXX, XXX) Xth XXXXXXXXX 20XX, Accepted Xth XXXXXXXXX 20XX
DOI: 10.1039/b000000x

Abstract: Nano-Ru/porous carbon composites were prepared by Ru/aerogels which were made through a reaction of resorcinol, formaldehyde and $RuCl_3 \cdot 3H_2O$. The specific surface area (SSA) measurement showed that there was a SSA maximum with the increase of Ru loading. The sample R_{Ru}=5 (mole percent) obtained the largest SSA value of 1970 $m^2 \cdot g^{-1}$ and the most homogeneous distribution of Ru nano-particle on the porous carbon surface. It also obtained the highest hydrogen adsorption value of 0.8 wt% (7.5 MPa) and 4.1 wt% (4 MPa) at 298 and 77 K respectively. Considering the H_2 compressed in pores, the corresponding total value reached up to 1.4 wt% (P=7.5 MPa) and 6.3 wt% (P=6.5 MPa) at 298 and 77 K respectively. Compared with porous carbon, the Ru/porous carbon composites had an obvious adsorption increase under same SSA condition at 298 K, which were contributed by the hydrogen spillover of Ru. The calculated contribution rate for the hydrogen adsorption was 38%. However, the spillover effect also brought a hysteresis phenomenon during hydrogen desorption as the hydrogen spilled from hydride into carbon matrix needed lower pressure to move and release.

Introduction

Many methods are presented to prepare porous carbon materials like chemical activation method,[1-3] carbonide reduction process[4-7] and polymer carbonization.[8, 9] As their good conductivity, large specific surface area (SSA) and big pore volume, they are usually used as electrode of supercapacitor [10-12], catalyst support,[13, 14] and especially they are wildly researched in hydrogen adsorption.[2, 3, 15-17] Among the characteristics of porous carbon materials, the SSA of porous carbon is very important parameter to evaluate its hydrogen storage ability. However, the limitation on the preparation of porous carbon with huge SSA has confined the hydrogen storage increase for porous carbon. [18] Therefore, a strategy of supporting catalysts on the porous carbon is introduced to enhance hydrogen storage, namely utilizing the spillover effect of catalyst to decompose H_2 molecular into hydrogen atom to make hydrogen store into materials.[19-23] There are many composites of porous carbons with catalysts (e.g. Pt, Pd, Ni, Co) have been prepared and applied in hydrogen storage.[24-28] Chen et al[29] reported the hydrogen storage of pristine AC with SSA value of 3300 $m^2 g^{-1}$, graphene sheet (GS)/AC and Pd-GS/AC were 0.63, 0.55 and 0.82 wt% at 289 K/8 MPa respectively. It was clearly found that the H_2 uptake of Pd-GS/AC was nearly 49% more than that of the GS/AC samples. Authors excluded the hydrogen storage of Pd and found that the H_2 physisorption of all samples strongly depended on the porosity of AC, and the enhanced H_2 uptake could be attributed to the contribution of the AC receptor via the hydrogen spillover effect. Huang et al[30] prepared cobalt-embedded ordered mesoporous carbon (OMC-Co) of which the hydrogen capacities was 0.45 wt%, more than two times of OMC At 298 K/5.5 MPa. The contribution of hydrogen spillover effect is obvious. R.T. Yang et al[31] reported that the hydrogen storage capacity of Pt-AX21 was enhanced to 1.2 wt % at 298 K/10 MPa. Furthermore, the isotherm was totally reversible and rechargeable at 298 K. To the catalysts obtaining hydrogen spillover effect, their particle size is expected to be as smaller as possible to increase the catalytic sites and hydrogen adsorption dynamic. Commonly, catalysts are introduced onto the surface of carbon support after the activation process. However, this strategy usually reduces the SSA of porous carbon because some micro- and nano-pores will be blocked up by catalyst particles.[32] Therefore, it is urgent to find a way to prepare porous carbon materials equipped with a homogenous catalyst dispersion and a rich porous structure which is not covered by catalysts unexpectedly to get an increasing available SSA. In additionally, even though many catalysts with hydrogen spillover have be reported, it is rare to evaluate the actual contribution of catalysts to the enhancement in hydrogen storage. In this work, spillover contribution to hydrogen storage will be discussed in detail.

Among those many carbon materials, carbon aerogels derived from organic aerogels synthesized by resorcinol and formaldehyde have been wildly researched as hydrogen adsorption agent,[33-36] because they have unique properties, such as controllable mass densities, continuous porosities, and high SSA. In this paper, a series of composite containing carbon aerogels and nano ruthenium (Ru) particles are prepared and

applied in hydrogen storage. The result shows that a large SSA can be obtained even after Ru being loaded , and the Ru particles with a highly uniform distribution loaded on the carbon aerogels enhance the hydrogen storage effectively.

Experimental

Synthesis of Ru/aerogel

The mole ratio of resorcinol to formaldehyde was limited to 1:2. Different mass of $RuCl_3.3H_2O$ was used as initiator. In the typical preparation of aero-gel, resorcinol (4.4g) was precisely weighted and solved in 8 ml deionized water, and then ultrasonically agitated for 10 min. The following was to slowly drop the formaldehyde (5.6 ml, 37% of contents) into the solution and it was supersonically agitated for another 10 min to mix regents completely. After above processes, it was kept at different temperatures for different time, namely, room temperature for 1day, 50 ℃ for 1 day and 90 ℃ for 3 days. Then the samples were immersed in acetone for 1 day to replace water produced in polycondensation process. Finally, it was dried in 80 ℃ at vacuum.

Carbonization and activation

Ru/carbon was prepared by carbonization of Ru/aerogel at 850 ℃ for 2 h in a flow of Ar in 100ml·min^{-1}. The Ru/carbon was subjected to activation by KOH at 850℃ for another 2h. Herein, the mass ratio of KOH to Ru/carbon is 4:1. After cooling down to room temperature, it was washed by deionized water for 3 times and then dried at 80 ℃. Herein, the Ru/porous carbon composites were denoted as R_{Ru} (R_{Ru} = C×100/R, C and R is mole fraction of $RuCl_3$ and resorcinol respectively).

Hydrogen storage measurement

All samples were measured in powder and their hydrogen-uptake measurements were carried out by Sieverts apparatus. The detailed on the calculations and measurements were shown in a previous paper.[37] The hydrogen adsorption was mainly measured at 293 K and 77 K. The physisorption of an empty sample cell was found to have a great influence on the final measurement. In this paper, all displayed hydrogen adsorption values was that the physisorption of empty sample cell was excluded.

Characterization methods

The morphologies and energy dispersive Spectroscopy (EDS) analysis of all samples were observed by field emission scanning electron microscopy (FE-SEM), JSM-6700F. The specific surface area (SSA) and pore volume were calculated by N_2 adsorption-desorption measurements, which were carried out on an ASAP 2020 surface area and porosity analyzer device. X-ray diffraction (XRD) characterization of the samples was carried out on XpertPRO X-ray diffractometer with Cu Kα radiation (λ=0.15444 nm).

Results and discussion

Firstly, the XRD test was conducted on aerogel, the Ru/carbon and the Ru/porous carbon samples with a content of R_{Ru}=5 to disclose the state of Ru. As seen from **fig. 1a**, Ru had been reduced by formaldehyde in the process of aerogel reaction. After

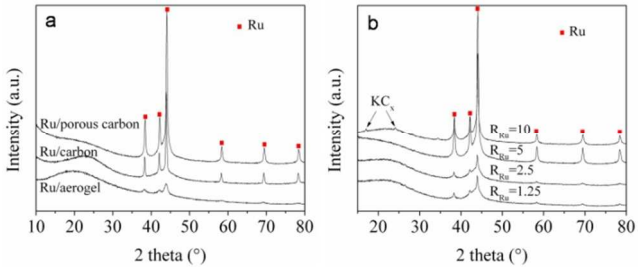

Fig.1 XRD spectrum of (a) different processing states of R_{Ru}=5 and (b) Ru/porous carbons with different Ru loadings

carbonization and activation, Ru still existed in pure metallic state. Fig.1b shows the XRD spectrum of four Ru/porous carbon composites with different Ru contents. Clearly, Ru existed in metallic state in all samples. Except for two peaks of KC_x (x=8, 9) appeared in the XRD spectrum of sample R_{Ru}=10, other three samples obtained smoothly broad peak in a range of 2θ=20~30°. Herein, the KC_x (x=8, 9) phase came from the intercalation of alkalis after the thermochemistry activation. In most reports, usually the carbon materials was amorphous and difficult to determine the KC_x phase. Whereas, some theoretical studies revealed that intercalation of alkalis into graphite structure could improve the hydrogen storage,[38, 39] and the effect on the hydrogen storage of KC_x will be discussed in the following.

Fig.2 (a-d) displays four back scattered electron (BSE) images of Ru/porous carbon. It is found that the carbon particle morphologies are different from each other. With the increase of R_{Ru}, the carbon particle size increases firstly and then decreases(fig.2e). Among all samples, the sample R_{Ru}=5 and R_{Ru}=10 have an uniform morphology with a carbon particle size of ca. 2μm. The sample R_{Ru}=1.25 and R_{Ru}=2.5 obtain a cross-linked structure and the sample R_{Ru}=2.5 obtains a bulk morphology with the biggest particle size of ca. 20μm. It demonstrates that the content of Ru at R_{Ru}=2.5 is a critical point to form cross-linked particles or even particles. As analyzed by XRD, Ru had been reduced by formaldehyde accompanied by the formation of aerogel, and then it served as growth nucleus in the formation of aerogel. The more Ru was reduced, the more nucleus sites appeared, and the smaller the aerogel particle size was. This is the reason why aerogels obtain different morphologies. Fig.2e (red line) shows the statistic number of Ru nanoparticles. To these four samples, the sample R_{Ru}=5 has the most Ru nanoparticles with a homogenous particle size of ca. 40 nm dispersing on the carbon surface. Whereas, the R_{Ru}=1.25 and R_{Ru}=2.5 samples have few Ru nanoparticles dispersing on the carbon surface. Even though the sample R_{Ru}=10 has a biggest $RuCl_3$ loading, Ru particles have aggregated into big cluster ultimately, as shown in fig.2d. The high light region marked by red cross in fig.2c is Ru particle which has been confirmed by EDS. These analysis and observation suggest that the Ru content can greatly affect the morphology of aerogel and the distribution of Ru nanoparticles. Additionally, the yields of samples after different process and the loading rates of Ru are listed in **table 1**. It is clearly seen that all yields increase with the increase of Ru loadings. The loading rate of Ru is a weight ratio of the actual loading of Ru to the final Ru/porous carbon weight.

According to above analysis, the growth mechanism of aerogel and preparation of Ru/porous carbon were displayed in **fig. 3**.

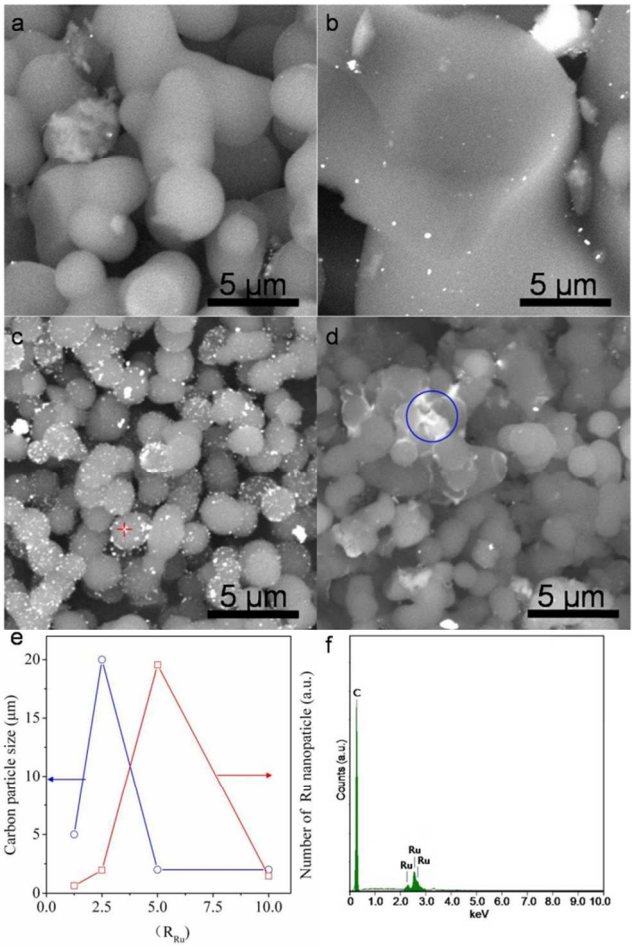

Fig.2 BSE images of Ru/porous carbon. (a) R_{Ru}=1.25,(b) R_{Ru}=2.5,(c) R_{Ru}=5, (d) R_{Ru}=10, (e) the carbon particle size distribution (blue) and the statistic number of Ru nanoparticles (red), (f) EDS patterns of particle marked in sample R_{Ru}=5

Table 1 The yields of samples after different process ,the loading rate of Ru and the hydrogen adsorption values at different temperatures.

Samples	Carbonization Yield/%	Activation yield /%	Total yield/%[c]	Ru wt%	H_2 wt% 298 K	H_2 wt% 77K
R_{Ru}=1.25	53.6	64.8	34.8	2.1	0.52	3.3
R_{Ru}=2.5	53.6	66.1	35.4	4.1	0.58	3.7
R_{Ru}=5	53.5	69.2	37.0	7.7	0.81	4.2
R_{Ru}=10	53.8	68.7	37.0	15	0.39	2.8

Firstly, Ru^{3+} ions were reduced by formaldehyde and Ru nanoparticles have formed, which had been proved by XRD analysis. At the same time, the resorcinol and formaldehyde reacted. Then the composite of Ru/aerogel formed and grew gradually. However, the Ru nanoparticles were embedded inside of aerogel in this section. As seen shown in fig.3a, there was no Ru dispersing on the aerogel surface. After carbonization and activation, aerogel had changed into porous carbon. Ru nanoparticles dispersed on the surface of carbon in big size (fig.3b) and small size (fig.3d), of which big size should attribute to the aggregation and growth of small ones at high temperature. Fig.3c shows the BSE image of a section of Ru/porous carbon. It is clearly seen that Ru nanoparticles not only disperse on the surface of porous carbon but also exists inside of porous carbon. The preparation schematic is shown in fig.3e.

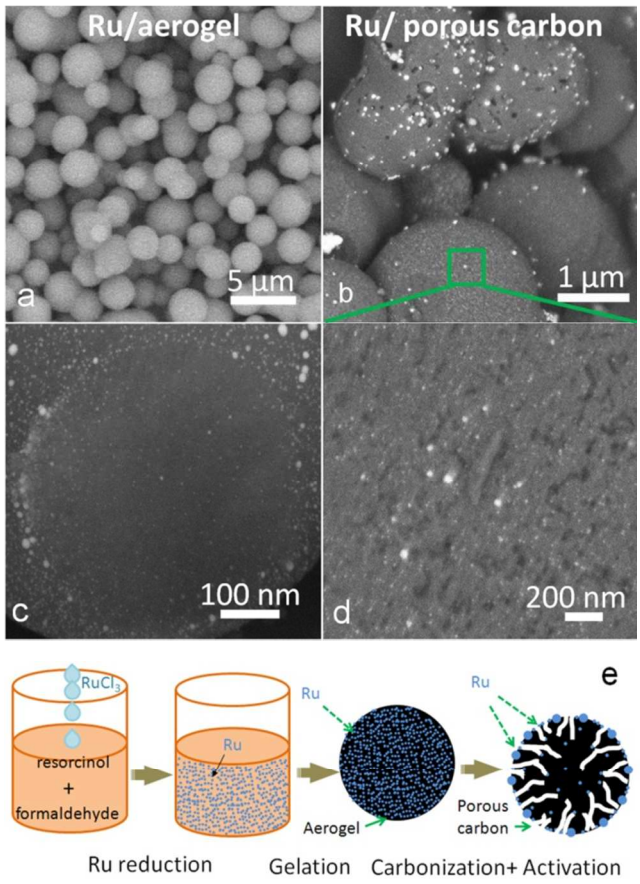

Fig.3 BSE images of (a) original Ru/aerogel of R_{Ru}=5, (b) activated Ru/porous carbon of R_{Ru}=5, (c) section of Ru/porous carbon of R_{Ru}=5, (d) high resolution image of surface(□ in fig. 3b), (e) preparation schematic of Ru/carbon aerogel.

Fig.4a shows the N_2 adsorption-desorption isotherm of the four activated Ru/porous carbon samples, and they all belongs to I-type adsorption. The result shows that R_{Ru}=5 sample obtains the biggest SSA value of 1970 $m^2 \cdot g^{-1}$ calculated by Brunauer–Emmett–Teller (BET) model and pore volume of 1.05 $cm^3 \cdot g^{-1}$ calculated by Barrett–Joyner–Halenda (BJH) model (fig. 4b). The SSA value of R_{Ru}=1.25, R_{Ru}=2.5 and R_{Ru}=10 is 1496, 1758 and 1342 $m^2 \cdot g^{-1}$ respectively, and the pore volume is 0.79, 0.93 and 0.74 $cm^3 \cdot g^{-1}$ respectively.

These four composites of Ru/porous carbon were employed as adsorbents to determine their hydrogen storage property. **Fig. 5(a, b)** show the hydrogen storage isotherm of four samples with different Ru contents at 298 and 77 K, and their hydrogen storage values measured at different temperature were listed in table 1. As a whole, the hydrogen storage at 298 K has an obvious distinction among these samples. The sample R_{Ru}=5 obtains the highest hydrogen adsorption value reaching up to 0.81 wt% at 7.5 MPa. Compared with pure carbon with a close or bigger SSA[9], the sample R_{Ru}=5 has an obvious enhancement of hydrogen adsorption which should be attributed to the spillover effect of Ru nanoparticles.[19, 40] Additionally, in these four hydrogen desorption isotherms, they all have displayed a phenomenon of hysteresis at range of low pressure. To the sample R_{Ru}=5, 0.11 wt% of hydrogen has not been released when the hydrogen pressure decreases to 0.01MPa, which is higher than the adsorption value

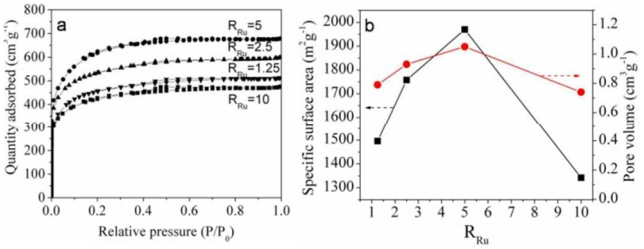

Fig.4 (a) N_2 adsorption-desorption isotherm of four activated Ru/porous carbon samples, (b) the relationship between SSA or pore volume and Ru loading.

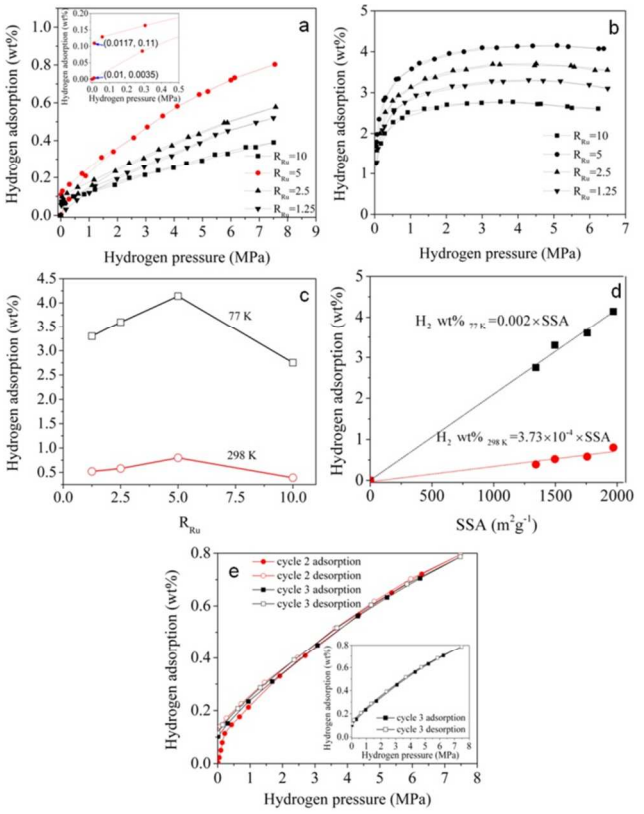

Fig.5 The hydrogen adsorption isotherm of Ru/porous carbon at (a) 298 K and (b) 77 K; (c) the relationship between the hydrogen adsorption and Ru loading at 298 and 77 K; (d) the linear correlation between the hydrogen adsorption and SSA at 298 and 77 K; (e) cyclic hydrogen adsorption measurements of the sample R_{Ru}=5 after the first test (● in fig.5a), (insert) the third cyclic measurement.

(0.004wt%) at same hydrogen pressure insert of fig.5a. Herein, there is 0.107 wt% of hydrogen having not been released. It is known that Ru has ability to split hydrogen molecules into atoms and then forms hydride like other transition metal (e.g. Pd, Pt). With the assumption of H:Ru=1,[41-43] the hydrogen storage in metallic Ru is 0.98 wt%. In this work, the sample R_{Ru}=5 contains 7.7 wt% of Ru loaded in porous carbon, thus Ru nanoparticles can store 0.075 wt% of hydrogen at most. Where is the residual 0.032 wt% of hydrogen stored? To the hydrogen storage of metal/porous carbon composites, a storage mechanism is illustrated in **fig.6a**. Hydrogen molecules mainly be stored in pores (as compressed hydrogen gas) or on carbon surface (as adsorbed hydrogen). When hydrogen molecules meet the Ru metallic particles, they will be splitted into hydrogen atoms and then the atoms can diffuse into metal to form metallic hydride and further, the hydrogen atoms in the hydride can go into carbon matrix (intercalated hydrogen) at the drive force of high pressure of hydrogen gas in tank. During hydrogen desorption, the hydrogen adsorbed on carbon surface and in pores can be released easily with the decrease of pressure. However, the hydrogen atoms in metal particles and carbon matrix are difficult to go out. Therefore, we considered that the residual 0.0315 wt% of hydrogen should be stored in carbon matrix. This part of hydrogen needs lower pressure to move and desorb and then a hysteresis loop was formed as shown in the insertion of fig.5a. This hysteresis phenomenon had been reported in many researches.[44-47] Li et al measured out of 0.1 wt% of hydrogen hysteresis desorption at 0.1 MPa for 5.6 wt% Pt/AX-21, and they also confirmed that about 0.015 wt% H was chemically adsorbed by the 5.6 wt% Pt according to Pt:H=1.[48] Similarly, Saha et al[24] had loaded 5 wt% Pt on ordered mesoporous carbon (OMC) and the extension desorption curve displayed that ca. 0.03wt% hydrogen had not been desorbed at near zero pressure, as shown in fig. 6b. Excluded about 0.013 wt% of hydrogen stored in 5 wt% Pt (calculated according to the data tested by Li et al[48]), therefore, another 0.017 wt% H should be stored in carbon matrix near metal catalyst.

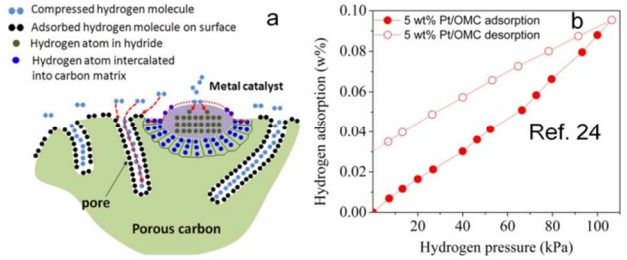

Fig.6 (a) the hydrogen storage sketch for metal/porous materials composite. (b) Hydrogen adsorption/desorption isotherms on 5 wt% Pt/OMC at low pressures and 298 K[24].

At low temperature 77 K, as seen from fig.5b, the saturation hydrogen adsorption value for the sample R_{Ru}=10 is only 2.75 wt%, which is the lowest. The values for sample R_{Ru}=1.25 and R_{Ru}=2.5 are of 3.3 and 3.6 wt% respectively. The sample R_{Ru}=5 obtains the highest saturation value of 4.1 wt%. Fig. 5c shows that collection of the hydrogen adsorption values at 298 and 77 K. It is found that they have similar trend with the SSA. Herein, the typical sample R_{Ru}=10 with KCx phase shows the lowest hydrogen adsorption, indicating that the KCx basically has no contribution to the total hydrogen storage. For the true physisorption of activated carbon at 77 K, Kabbour et al[49] gave an experimental rule about the relationship between the hydrogen adsorption of porous materials and their SSA, namely, 500 m^2·g^{-1} of SSA contributes 1 wt% to the hydrogen adsorption (H_2 wt%=2×10^{-3}×SSA), but the rule at 298 K had rarely been presented, and the contribution rate of catalyst with spillover effect was even rarely analyzed. Our previous research had proved that this rule is right basically at 77 K, and also the rule at 298 K had been presented as H_2 wt%=2.33×10^{-4}×SSA [9]. In this work, the equation of Ru/porous carbon composites has changed into H_2 wt%=3.73×10^{-4}×SSA. Clearly, the Ru/porous carbon has bigger slope value than pure activated carbon at 298 K, indicating that Ru indeed increases the hydrogen adsorption by its hydrogen spillover effect under same conditions of SSA and pressure. The

contribution rate (R) is about 38% which is calculated by equation (1).

$$R=\frac{H_2wt\%_{\text{Ru-porous carbon}}-H_2wt\%_{AC}}{H_2wt\%_{\text{Ru-porous carbon}}}\times 100\% \quad (1)$$

Herein, R is the contribution rate of Ru to hydrogen adsorption, H_2 wt%Ru-porous carbon and H_2 wt%AC [9] is the calculated hydrogen adsorption values at same SSA using the two hydrogen formulas at 298 K mentioned above.

The hydrogen adsorption of Ru/porous carbon composites tested at 77 K still consist with the rule of H_2 wt%=$2\times10^{-3}\times$SSA. It seems that the hydrogen spillover effect has an unobvious contribution to the total hydrogen adsorption.

In order to evaluate the cyclic hydrogen adsorption performance of the sample R_{Ru}=5, another two measurements after the first measurement were carried out. Their isotherms are shown in fig.5e. Before the second measurement, the sample was degassed fully. As seen from fig.5e, the second hydrogen adsorption/desorption isotherm (red line) is similar to the first one (red line in fig.5a), and they all have hysteresis loop. The hydrogen adsorption value is 0.8 wt% at 7.5 MPa for the second measurement, which is little less than the first one (0.81wt%). After the second cyclic measurement, the third measurement was directly carried out without degassing. The test result shows that the hydrogen adsorption/desorption isotherm basically is same to the desorption curve of the second cyclic measurement and it is fully reversible (insert in fig.5e). It suggests that physisorption contributes to all hydrogen adsorption. Even though the displayed hydrogen adsorption value is 0.79 wt% for the third cyclic measurement, its start hydrogen adsorption value is 0.1 wt%, therefore, the real adsorption is 0.69 wt%. This value is high than that of pure AC (ca. 0.6 wt% at 7.5MPa) with bigger SSA.[9, 29, 32, 48] The increase in hydrogen storage should be attributed to the hydrogen spillover effect.

In addition to the effect of SSA, the pore volume also significantly contributes to hydrogen storage. According to Yaghi et al.,[50] the total hydrogen storage is composed of two parts: (1) the surface adsorption and (2) the bulk density of hydrogen in the pores of the adsorbent (compressed hydrogen). Therefore, $M_{total}=M_{adsorption}+\rho_{H2}\times V_{pore}$, where $M_{adsorption}$ is the surface hydrogen adsorption; ρ_{H2} is the compressed hydrogen density at 298 or 77 K; V_{pore} is the pore volumes of carbon materials. The compressed hydrogen density data derives from the American National Institute of Standards and Technology. As shown in **fig. 7 (a, b)**, The pore volume of 1.05 $cm^3\cdot g^{-1}$ for the sample

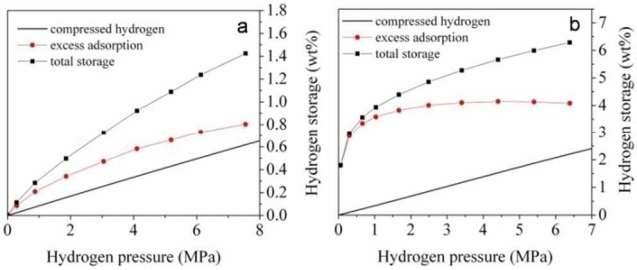

Fig.7 The hydrogen storage isotherms of sample R_{Ru}=5 at (a) 298 K and (b) 77 K. The (●) is the adsorption of sample R_{Ru}=5; the solid line indicates the amount of pure H_2 gas stored in the pores ($\rho_{H2}\times V_{pore}$); the (■) is the summation of the adsorption and the gas stored in the pores.

R_{Ru}=5 contributes to the total hydrogen adsorption up to approximately 0.57 wt% (7.5 MPa) and 2.2 wt% (6.5 MPa) at 298 and 77 K respectively. The total values reached up to 1.4 wt% (7.5 MPa) and 6.3 wt% (6.5 MPa) at 298 and 77 K respectively.

The hydrogen adsorption heat of the sample R_{Ru}=5 were also measured. **Fig.8** shows the hydrogen adsorption curve. Its original adsorption heat reaches up to 8.5 $kJ\cdot mol^{-1}$, which is higher than that of multiwalled carbon nanotubes (1.7 $kJ\cdot mol^{-1}$),[51] MOF-177 (4 $kJ\cdot mol^{-1}$) [50] or activated carbon AX-21 (6.4 $kJ\cdot mol^{-1}$). [51] The calculation method is as follows.[51]

$$-\Delta H=-R\left[\frac{d\ln P}{d(1/T)}\right]_n \quad (2)$$

Where ΔH is the adsorption heat (kJ·mol-1), P is the hydrogen pressure (MPa), T is the operation temperature (K) and R is the gas constant (8.314 $J\cdot K^{-1}\cdot mol^{-1}$).

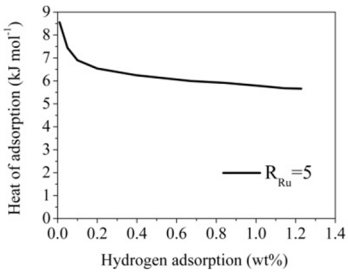

Fig.8 Hydrogen adsorption heat of the sample R_{Ru}=5

Conclusions

Aerogels with different Ru loadings were prepared by a reaction of resorcinol, formaldehyde and $RuCl_3\cdot 3H_2O$. The determination results showed that the Ru^{3+} was reduced into nano Ru firstly, and then the nano Ru catalyzed the formation of aerogel particles. After the carbonization and activation, the sample R_{Ru}=5 obtained the largest SSA value of 1970 $m^2\cdot g^{-1}$ and the most even distribution of Ru nano-particle on carbon surface. Finally, its hydrogen adsorption had reached up to 0.81 wt% (7.5 MPa) and 4.1 wt% (6.5 MPa) at 298 and 77 K respectively. Its original hydrogen adsorption had heat reached up to 8.5 $kJ\cdot mol^{-1}$. Compared with porous carbon, the hydrogen adsorption of Ru/porous carbon composites had been enhanced by the hydrogen spillover effect of Ru at 298 K. The calculation results show that this effect could obviously contribute 38% to the hydrogen adsorption. Additionally, the spillover effect also made a hysteresis phenomenon during hydrogen desorption, because the hydrogen spilled from hydride into carbon matrix needed lower pressure to diffuse and desorb.

Acknowledgements

This work was supported by the China Postdoctoral Science Foundation (No. 2012M521760).

Notes and references

State Key Laboratory for Mechanical Behavior of Materials, School of Material Science and Engineering, Xi'an Jiaotong University, Xianning west road No. 28, Xi'an 710049,PR China

TEL:+86 -29-82664602
E-mail: ynliu@mail.xjtu.edu.cn (Yongning Liu)

1 M. M. d. Castro, M. Martez-Escandell, M. Molina-Sabio and F. Rodruez-Reinoso, *Carbon*, 2010, **48**, 636.
2 H. Y. Tian, C. E. Buckley, S. B. Wang and M. F. Zhou, *Carbon*, 2009, **47**, 2128.
3 H. L. Wang, Q. M. Gao and J. Hu, *J. Am. Chem. Soc.*, 2009, **131**, 7016.
4 Y. Gogotsi, A. Nikitin, H. Ye, W. Zhou, J. E. Fischer, B. Yi, H. C. Foley and M. W. Barsoum, *Nat. Mater.*, 2003, **2**, 591.
5 J. Chmiola, C. Largeot, P.-L. Taberna, P. Simon and Y. Gogotsi, *Science*, 2010, **328**, 480.
6 Y. Korenblit, M. Rose, E. Kockrick, L. Borchardt, A. Kvit, S. Kaskel and G. Yushin, *ACS Nano*, 2010, **4**, 1337.
7 A. Jänes, T. Thomberg and E. Lust, *Carbon*, 2007, **45**, 2717.
8 Y. Chen, X. Cao, H. Zhu and Y. Liu, *Int. J. Hydrogen Energy*, 2012, **37**, 7629.
9 Y. Chen, H. Zhu and Y. Liu, *Int. J. Hydrogen Energy*, 2011, **36**, 11738.
10 V. Ruiz, C. Blanco, M. Granda and R. Santamaría, *Electrochim. Acta*, 2008, **54**, 305.
11 S. Bose, T. Kuila, A. K. Mishra, R. Rajasekar, N. H. Kim and J. H. Lee, *J. Mater. Chem.*, 2012, **22**, 767.
12 F. Zhou, Q. Liu, D. Kang, J. Gu, W. Zhang and D. Zhang, *J. Mater.s Chem. A*, 2014, **2**, 3505.
13 P. R. Shukla, S. Wang, H. Sun, H. M. Ang and M. Tadé, *Appl.Catal. B- Environ.*, 2010, **100**, 529.
14 N. Mahata, O. S. G. P. Soares, I. Rodríguez-Ramos, M. F. R. Pereira, J. J. M. Órfão and J. L. Figueiredo, *Appl. Catal. A-Gen.*, 2013, **464–465**, 28.
15 H. Jin, Y. S. Lee and I. Hong, *Catal. Today*, 2007, **120**, 399.
16 M. Jordá-Beneyto, D. Lozano-Castelló, F. Suárez-García, D. Cazorla-Amorós and Á. Linares-Solano, *Microporous Mesoporous Mater.*, 2008, **112**, 235.
17 M. Jord-Beneyto, F. Sulez-Garcd, D. Lozano-Castell, D. Cazorla-Amorm and A. Linares-Solano, *Carbon*, 2007, **45**, 293.
18 V. Fierro, A. Szczurek, C. Zlotea, M. J. F., M. T. Izquierdo, A. Albiniak, M. Latroche, G. Furdin and A. Celzard, *Carbon*, 2011, **48**, 1902.
19 Y. Li and R. T. Yang, *J. Am. Chem. Soc.*, 2006, **128**, 8136.
20 Y. Li and R. T. Yang, *AIChE J.*, 2008, **54**, 269.
21 L. Wang and R. T. Yang, *Energy Environ. Sci.*, 2008, **1**, 268.
22 Y. Wang, K. Wang, C. Guan, Z. He, Z. Lu, T. Chen, J. Liu, X. Tan, T. T. Yang Tan and C. M. Li, *Int. J. Hydrogen Energy*, 2011, **36**, 13663.
23 B. D. Adams, C. K. Ostrom, S. Chen and A. Chen, *J. Phys. Chem. C*, 2010, **114**, 19875.
24 D. Saha and S. Deng, *Langmuir*, 2009, **25**, 12550.
25 L. Zubizarreta, J. A. Menéndez, N. Job, J. P. Marco-Lozar, J. P. Pirard, J. J. Pis, A. Linares-Solano, D. Cazorla-Amoro and A. Arenillas, *Carbon*, 2010, **48**, 2722.
26 Y. Yang, C. M. Brown, C. Zhao, A. L. Chaffee, B. Nick, D. Zhao, P. A. Webley, J. Schalch, J. M. Simmons, Y. Liu, J.-H. Her, C. E. Buckley and D. A. Sheppard, *Carbon*, 2011, **49**, 1305.
27 L. Zubizarreta, J. A. Menéndez, J. J. Pis and A. Arenillas, *Int. J. Hydrogen Energy*, 2009, **34**, 3070.
28 Z. Wang and R. T. Yang, *J. Phys. Chem. C*, 2010, **114**, 5956.
29 C.-H. Chen, T.-Y. Chung, C.-C. Shen, M.-S. Yu, C.-S. Tsao, G.-N. Shi, C.-C. Huang, M.-D. Ger and W.-L. Lee, *Int. J. Hydrogen Energy*, 2013, **38**, 3681.
30 C.-C. Huang, Y.-H. Li, Y.-W. Wang and C.-H. Chen, *Int. J. Hydrogen Energy*, 2013, **38**, 3994.
31 R. T. Yang and Y. Wang, *J. Am. Chem. Soc.*, 2009, **131**, 4224.
32 L. Wang and R. T. Yang, *Carbon*, 2012, **50**, 3134.
33 H. Y. Tian, C. E. Buckley, D. A. Sheppard, M. Paskevicius and N. Hanna, *Int. J. Hydrogen Energy*, 2010, **35**, 13242.
34 F.-M. Kong, J. D. LeMay, S. S. Hulsey, C. T. Alviso and R. W. Pekala, *J. Mater. Res.*, 1993, **8**, 3100.
35 H. Kabbour, T. F. Baumann, J. H. Satcher, A. Saulnier and C. C. Ahn, *Chem. Mater.*, 2006, **18**, 6085.
36 K. Y. Kang, B. I. Lee and J. S. Lee, *Carbon*, 2009, **47**, 1171.
37 Y. Chen, Q. Liu, Y. Yan, X. Cheng and Y. Liu, *Carbon*, 2010, **48**, 714.
38 Z. H. Zhu, G. Q. Lu and S. C. Smith, *Carbon*, 2004, **42**, 2509.
39 D. Saha, C. I. Contescu and N. C. Gallego, *Langmuir*, 2012, **28**, 5669.
40 Y. Li and R. T. Yang, *J. Am. Chem. Soc.*, 2006, **128**, 726.
41 M. Lindroos, H. Pfnür, P. Feulner and D. Menzel, *Surf. Sci.*, 1987, **180**, 237.
42 Y. K. Sun and W. H. Weinberg, *Surf. Sci. Lett.*, 1989, **214**, L246.
43 M. Lindroos, H. Pfnür and D. Menzel, *Surf. Sci.*, 1987, **192**, 421.
44 G. Ferey, M. Latroche, C. Serre, F. Millange, T. Loiseau and A. Percheron-Guegan, *Chem. Commun. (Cambridge, U. K.)*, 2003.
45 X. Zhao, B. Xiao, A. J. Fletcher, K. M. Thomas, D. Bradshaw and M. J. Rosseinsky, *Science*, 2004, **306**, 1012.
46 H. Kobayashi, M. Yamauchi, H. Kitagawa, Y. Kubota, K. Kato and M. Takata, *J. Am. Chem. Soc.*, 2008, **130**, 1818.
47 H. Kobayashi, M. Yamauchi, H. Kitagawa, Y. Kubota, K. Kato and M. Takata, *J. Am. Chem. Soc.*, 2008, **130**, 1828.
48 Y. Li and R. T. Yang, *J. Phys. Chem. C*, 2007, **111**, 11086.
49 H. Kabbour, T. F. Baumann, J. H. Satcher, A. Saulnier and C. C. Ahn, *Chem. Mater.*, 2006, **18**, 6085.
50 H. Furukawa, M. A. Miller and O. M. Yaghi, *J. Mater. Chem.*, 2007, **17**, 3197.
51 L. Zhou, Y. Zhou and Y. Sun, *Int. J. Hydrogen Energy*, 2004, **29**, 475.